Atomic bond breaking behavior during grain boundary fracture in a C-segregated Fe grain boundary

Naoki Miyazawa*, Masataka Hakamada and Mamoru Mabuchi

Graduate School of Energy Science, Kyoto University, Yoshidahonmachi, Sakyo, Kyoto 606-8501, Japan

* Corresponding author. E-mail: miyazawa.naoki.37c@st.kyoto-u.ac.jp

First-principles fully relaxed tensile tests were performed on a C-segregated Fe Σ3 (111)/[$1\bar{1}0$] symmetrical tilt grain boundary (GB) to investigate the breaking behavior of C–Fe bonds during tensile straining. Fe atoms around a C atom moved obliquely to the tensile direction, and C–Fe bonds stretched in the tensile direction without premature bond breaking. Analyses of the electronic states during deformation showed that a variation in the charge density at the bond critical point was much larger for the C-Fe bond than for the P-Fe bond and that the C atom exhibited larger variations of *s* and *p* states involved in the covalent-like characteristics than the P atom. It is suggested that these lead to a high mobility of the C-Fe bonds. On the other hand, first-principles shear tests on the Fe GB imply that C-segregated Fe GB toughening is not associated with increased crack blunting by dislocation emission.

Keywords: first-principles calculation; fracture; grain boundary; segregation, iron

Introduction

Segregation of impurities at grain boundaries (GBs) often induces embrittlement or toughening/strengthening of materials in which GB fracture occurs. The origins of enhanced embrittlement by segregation have been extensively investigated from an electronic viewpoint [1], and explanations of embrittlement have been provided, such as a bond mobility model [2], a decohesion model [3], size effects [4,5] and local stress concentrations [6]. In the bond mobility model, embrittlement is caused by limited bond

mobility arising from covalent bonding between impurities and neighboring host atoms [2]. For example, the covalent-like characteristics of P–Fe induce premature atomic bond breaking of P–Fe, resulting in enhanced embrittlement of Fe GBs by P segregation [7]. However, GB toughening or strengthening by segregation occurs in iron [8-11] and other materials [12,13] when the bonds between impurity atoms and neighboring host atoms are covalent. Thus, both the bond mobility model of GB embrittlement and the explanation for GB toughening/strengthening by segregation are associated with the covalent characteristics of the atomic bonds between impurity and host atoms, so the material responses cannot be only the result of covalency.

Thermodynamic analysis [14] is another approach to investigate segregation effects, where the tendency toward embrittlement or toughening can be estimated using state functions of the GB energy before deformation and the surface energy after fracture. The fracture energy for deformable materials tends to increase with increasing ideal brittle fracture energy, which is estimated assuming that the breaking of all atomic bonds is reversible [15]. However, not only reversible atomic bond breaking, but also irreversible atomic bond breaking occurs in fracture of deformable solids. Hence, irreversible atomic bond breaking may lead to GB toughening/strengthening on account of the covalent characteristics of the bonds.

Methodology

It is well known that C toughens or strengthens Fe GBs [16]. First-principles calculations of the effects of C on Fe GB cohesion have been performed [9,10,17-19]. Recently, first-principles fully relaxed tensile tests, in which a cell is first strained and then the atoms in the cell are fully relaxed, have been carried out for a more realistic description of tensile tests by first-principles calculations [7,20]. Irreversible atomic

bond breaking can be achieved by using this model. In the present work, first-principles fully relaxed tensile test simulations were performed on a C-segregated Fe Σ3 (111)/[$1\bar{1}0$] symmetrical tilt GB to investigate the breaking behavior of C–Fe bonds during tensile straining.

Geometry optimization calculations were performed using the Cambridge serial total energy package (CASTEP) [21] with ultrasoft pseudopotentials [22], and a 300-eV plane-wave cut-off was used to perform the first-principles calculations. A Monkhorst-Pack 6 × 4 × 2 *k*-point mesh and 0.1-eV-wide Gaussian smearing were used. The exchange–correlation interactions were treated using the spin-polarized version of the generalized gradient approximation within the Perdew–Burke–Ernzerhof functional [23]. The simulation conditions, such as the cut-off energy, sampling k-points, and Gaussian smearing, were determined on the basis of the previous studies [17,24].

A body-centered cubic Fe Σ3 (111)/[$1\bar{1}0$] tilt GB cell (clean GB) was used. The lattice parameter of the Fe cell was 0.2867 nm, which agrees adequately with the experimental value (0.2870 nm). The C atoms were placed at interstitial sites of the Fe GB in a C-segregated GB cell (Figure 1), which are the energetically most stable sites for C segregation [17]. The cell contained 36 Fe atoms for the clean GB, and 36 Fe atoms and two C atoms for the C-segregated GB. The initial cells were 0.405 nm × 0.702 nm × 1.489 nm [24]. The C concentration at the C-segregated GB was 3.8 at.%, assuming that the GB width was 1 nm. It has been experimentally showed that the C concentrations at the GB in Fe are in the range 3.0–14.4 at.% [25]. Also atom probe tomography revealed that the C concentrations at the GB in carbon-added Fe were about 2 at.% [26]. Thus, the C concentration at the GB in the C-segregated GB model in the present work is comparable with the concentrations in the experimental studies. A P-segregated Fe Σ3 (111)/[$1\bar{1}0$] tilt GB cell, which is the same as that in the previous

study [7], was also constructed for comparison with the C-segregated GB. After relaxing each cell, a 2% incremental uniaxial tensile strain was applied in the [111] direction (normal to the GB plane) to the cells for the first-principles fully relaxed tensile tests. All the atomic positions were relaxed based on Hellmann–Feynman forces until all of the forces were less than 0.03 eV/Å. The lattice dimensions in the GB plane were fixed during the calculations, ignoring the Poisson's ratio to simplify the calculations [6,27,28]. This step was iterated until the GB fractured. After convergence of the Hellman–Feynman forces, the total energies of the simulations cell were calculated, assuming they were zero before deformation.

First-principles shear tests were also performed by shifting the upper grain with respect to the lower grain of 1/20 of the coincidence site lattice (CSL) units in the (111) plane. The atoms in the two layers in the middle of each grain were fixed at their bulk positions during the geometry optimization, and the other atoms were allowed to relax [29,30]. The sliding was continued until energy reduction, where GB migration occurred.

Results and Discussion

The results of first-principles fully relaxed tensile tests are shown in Figure 2. The total energy of the simulation cell for the C-segregated GB was higher than that for the clean GB below 26% strain. For the C-segregated GB, the total energy decreased above 26% strain because of GB separation. On the other hand, for the clean GB, the total energy increased below 28% strain and decreased above 28% strain. As a result, the maximum value of the total energy for the C-segregated GB was lower than that for the clean GB, although the difference was small. Considering the stress (Figure 2(b)), the maximum stress for the C-segregated GB was a little larger than that for the clean GB,

indicating that the GB strength was enhanced by C segregation. Note that the stress decreased a little from 20% to 22% strain in the C-segregated GB, while such a decrease in the stress was not observed in the clean GB.

The charge density distributions for the $(1\bar{1}0)$ plane in the C-segregated GB are shown in Figure 3. The C and Fe atoms were strongly bonded because of the large charge density. However, the C1–Fe4 bond was broken from 20% to 22%. This corresponds to the fact that the stress decreased from 20% to 22% in the C-segregated GB. After breaking of C1–Fe4, the Fe4 atom moved almost parallel to the tensile direction with straining, and the Fe2 atom moved toward the space where the Fe4 atom had been located, whose direction of movement was oblique to the tensile direction by changing the Fe2–C1–Fe1 bond angle. Fe1 and Fe3 atoms also moved obliquely to the tensile direction by changing the Fe1–C1–Fe3 angle. Thus, the C–Fe bonds stretched in the tensile direction without premature bond breaking by changes in the Fe–C–Fe angles, except for the C1–F4 bond. Note that the Fe atoms around the C atom exhibited high bond mobility, despite the covalent-like characteristics of C–Fe as shown later. C–Fe bonding has spatial anisotropy, that is stronger vertical C–Fe bonding and weaker lateral C–Fe bonding [9]. The same trend was found in Cr–Fe bonding, which leads to enhanced Fe GB cohesion [11]. However, the origin of high bond mobility of covalent-like bonded C-Fe cannot be sufficiently explained only by the spatial anisotropy.

It is known that P is a strong embrittler of Fe GBs, although the Fe–P bond also exhibits covalent characteristics [7]. All of the Fe atoms around the P atom only moved parallel to the tensile direction in the P-segregated GB [7]. The calculation in the P-segregated GB was performed by ignoring the Poisson's ratio as well as that in the C-segregated GB, which indicates that the difference in bond mobility between C-Fe and P-Fe is not related to the calculation condition of ignoring the Poisson's ratio. Clearly,

the Fe atoms around the P atom have the limited bond mobility. Hence, it is worthwhile to investigate the origin of high bond mobility of C-Fe in comparison with the P-Fe. The effects of segregation on GB cohesion/decohesion can be classified into size effects and chemical effects [4,31-34]. Size effects tend to decrease the GB cohesion, whereas chemical effects tend to increase the GB cohesion [4,31-34]. Hence, the enhanced cohesion of Fe GBs by C segregation can be attributed to the chemical effects of C–Fe bonding. The partial densities of states (PDOSs) of the C1 atom in the C-segregated GB are shown in Figure 4. The PDOSs of the Fe2 and Fe4 atoms in the C-segregated GB are shown in Figure 5, where the inset of each figure shows the PDOSs at −13 to −10 eV of orbitals related to covalent-like bonding. Hybridization of C *s* and Fe *s* states, and C *p* and Fe *d* states occurred at −13 to −10 eV and −8 to −5 eV before straining, respectively, indicating that C–Fe bonds have covalent-like characteristics. The trend of covalent-like characteristics related to the *s* and *p* states of the C atom for C–Fe bonding is the same as that of the P atom for P–Fe bonding [7]. The hybridization in the Fe4 atom disappeared at 22% strain (Figure 5), corresponding to the bond breaking of C1–Fe4 occurring from 20% to 22% strain. Note that the peaks of the *s* and *p* states of the C1 atom, which are involved in the covalent-like characteristics of C–Fe bonds, gradually shifted toward the Fermi level with straining. The peaks of the *s* and *p* states that are involved in the covalent-like characteristics of P–Fe bonds also gradually shifted toward the Fermi level with straining (Figure 6). However, an inspection of Figures 4 and 6 reveals that the peak shift is larger for the C–Fe bonds than for the P–Fe bonds. Only a little charge transfer occurs between C and Fe atoms [10,18]. Similarly, charge transfer between P and Fe atoms was only a little from the population analysis (which is not shown in the present paper). Thus, the charge transfer does not play an important role in both the C-Fe and the P-Fe bonds. Therefore, it is suggested that the C

atom exhibits large variations of *s* and *p* states involved in the covalent-like characteristics than the P atom.

There is a close relation between topological properties of electronic charge density and solid state structures [35]. The characteristic topology of any scaler field is given in terms of its critical points, which are the zeros of the gradient of this field. In particular, the charge density at the bond critical point (BCP), which is a saddle point [35], is crucial for atomic bond breaking [36]. Figure 7 shows the charge density along the line normal to the C1–Fe4 bond passing through the BCP of C1–Fe4. Note that the charge density at the BCP decreases with straining despite the covalent-like characteristics of C1–Fe4. Finally, the curve of the charge density at the BCP becomes flat at 22% strain. The trend of charge density variation with straining for the C1–Fe4 bond is similar to that for the Fe–Fe bond in the clean Fe GB [37]. However, the variation in the charge density at the BCP with straining is significantly lower for the P–Fe bond [37]. Clearly, the C-Fe bond shows much larger variation in the charge density during deformation than the P-Fe bond. In addition, the C atom exhibits larger variations of *s* and *p* states involved in the covalent-like characteristics than the P atom, as shown in Figures 4 and 6. These are suggested to lead to the high bond mobility of C-Fe.

Blunting a sharp crack by emitting dislocations from its tip is another toughening mechanism [38]. Although it is difficult to precisely assess the dislocation emission by the first-principles calculations, a trend of the dislocation emission can be estimated by first-principles shearing tests. In the present paper, effects of C on the dislocation emission were estimated by first-principles shearing tests with the Fe GB cells. The results of the shearing test simulations showed that more energy is required for shear deformation with C addition (Figure 8). This suggests that C-segregated Fe GB toughening is not because of increased crack blunting by the dislocation emission

because C atoms hinder the dislocation emission. The hindered dislocation emission by C atoms is probably due to the covalent-like bonding of C-Fe. Let consider GB strengthening mechanisms by covalent bonds. In the case of low mobility of covalent bonds, like P-Fe bonds, GBs are embrittled as expected on the bond mobility model. However, when the mobility of covalent bonds is not reduced much, like C-Fe bonds, the embrittlement expected by the bond mobility model does not occur, and GBs are strengthened due to the strong interface adhesion caused by covalent bonding. It is important to note that a role of a covalent bond in grain boundary embrittlement or strengthening depends on its bond mobility. There are some limitations of the present calculation scheme, such as the GB investigated is only the Σ3 GB, no dislocations and cracks are generated, there are no natural defects of steps and facets at the GB plane, and the effects of lattice vibrations are not considered. However, the bond mobility of C–Fe will be relatively high in other Fe GBs as well, despite the limitations of the present calculations.

Conclusions

First-principles fully relaxed tensile tests were performed on a C-segregated Fe Σ3 (111)/$[1\bar{1}0]$ symmetrical tilt grain boundary (GB). Fe atoms around a C atom moved obliquely to the tensile direction without premature bond breaking. Thus, the C-Fe bonds showed a high bond mobility. A variation in the charge density at the bond critical point was large for the C-Fe bond and the C atom exhibited large variations of *s* and *p* states involved in the covalent-like characteristics. It is suggested that these lead to a high mobility of C-Fe bonds. On the other hand, it is implied from the first-principles shear tests on the Fe GB that C-segregated Fe GB toughening does not arise from increased crack blunting by dislocation emission.

References

[1] M. A. Gibson and C. A. Schuh, *A comparison of ab-initio calculations of embrittling potencies in binary metallic alloys*, Data in Brief 6 (2016), pp.143-148.

[2] R. Haydock, *The mobility of bonds at metal surfaces*, J. Phys. C 14 (1982), pp.3807-3816.

[3] R. Messmer and C. L. Briant, *The role of chemical bonding in grain boundary embrittlement*, Acta Metall. 30 (1982), pp.457-467.

[4] R. Schweinfest, A. T. Paxton and M. W. Finnis, *Bismuth embrittlement of copper is an atomic size effect*, Nature 432 (2004), pp.1008-1011.

[5] A. Y. Lozovoi, A. T. Paxton and M. W. Finnis, *Structural and chemical embrittlement of grain boundaries by impurities: A general theory and first-principles calculations for copper*, Phys. Rev. B 74 (2006), pp.155416.

[6] G. -H. Lu, Y. Zhang, S. Deng, T. Wang, M. Kohyama, R. Tamamoto, F. Liu, K. Horikawa, and M. Kanno, *Origin of intergranular embrittlement of Al alloys induced by Na and Ca segregation: Grain boundary weakening*, Phys. Rev. B 73 (2006), pp.224115.

[7] M. Yuasa and M. Mabuchi, *Bond mobility mechanism in grain boundary embrittlement: First-principles tensile tests of Fe with a P-segregated Σ3 grain boundary*, Phys. Rev. B 82 (2010), pp.094108.

[8] R. Wu, A. J. Freeman and G. B. Olson, *First principles determination of the effects of phosphorus and boron on iron grain boundary cohesion*, Science 265 (1994), pp.376-380.

[9] R. Wu, A. J. Freeman and G. B. Olson, *Effects of carbon on Fe-grain-boundary cohesion: First-principles determination*, Phys. Rev. B 53 (1996), pp.7504.

[10] P. Rez and J. R. Alvarez, *Calculation of cohesion and changes in electronic structure due to impurity segregation at boundaries in iron,* Acta Mater. 47 (1999), pp.4069-4075.

[11] R. Yang, D. L. Zhao, Y. M. Wang, S. Q. Wang, H. Q. and C. Y. Wang, *Effects of Cr, Mn on the cohesion of the γ-iron grain boundary,* Acta Mater. 49 (2010), pp.1079-1085.

[12] S. N. Sun, N. Kioussis and M. Ciftan, *First-principles determination of the effects of boron and sulfur on the ideal cleavage fracture in Ni3Al,* Phys. Rev. B 54 (1996), pp.3074-3078.

[13] J. Chen, Y. N. Xu, P. Rulis, L. Ouyang and W. Y. Ching, *Ab initio theoretical tensile test on Y-doped Σ = 3 grain boundary in a-Al_2O_3,* Acta Mater. 53 (2005), pp.403-410.

[14] J. R. Rice and J. S. Wang, *Embrittlement of interfaces by solute segregation,* Mater. Sci. Eng. A 107 (1989), pp.23-40.

[15] M. L. Jokl, V. Vitek, and C. J. McMahon Jr., *A microscopic theory of brittle fracture in deformable solids: A relation between ideal work to fracture and plastic work,* Acta Metall. 28 (1980), pp.1479-1488.

[16] K. Abiko, S. Suzuki, and H. Kimura, *Effect of carbon on the toughness and fracture mode of Fe-P alloys,* Trans. Jpn. Inst. Met. 23 (1982), pp.43-52.

[17] M. Yamaguchi, *First-principles study on the grain boundary embrittlement of metals by solute segregation: Part I. iron (Fe)-solute (B, C, P, and S) systems,* Metall. Mater. Trans. A 42 (2011), pp.319-329.

[18] J. R. Braithwaite and P. Rez, *Grain boundary impurities in iron*, Acta Mater. 53 (2005), pp.2715-2726.

[19] N. Hatcher, G. K. H. Madsen and R. Drautz, *Parameterized electronic description of carbon cohesion in iron grain boundaries*, J. Phys.: Condens. Matter 26 (2014), pp.145502.

[20] G. -H. Lu, S. Deng, T. Wang, and M. Koyama, *Theoretical strength of an Al grain boundary*, Phys. Rev. B 69 (2004), pp.134106.

[21] M. C. Payne, M. P. Teter, D. C. Allan, T. A. Arias and J. D. Joannopoulos, *Iterative minimization techniques for ab initio total-energy calculations: molecular dynamics and conjugate gradients*, Rev. Mod. Phys. 64 (1992), pp.1045.

[22] D. Vanderbilt, *Soft self-consistent pseudopotentials in a generalized eigenvalue formalism*, Phys. Rev. B 14 (1990), pp.7892.

[23] J. P. Perdew, K. Burke and M. Ernzerhof, *Generalized gradient approximation made simple*, Phys. Rev. Lett. 77 (1996), pp.3865.

[24] M. Yamaguchi, M. Shiga, and H. Kaburaki, *Grain boundary decohesion by impurity segregation in a nickel-sulfur system*, Science 307 (2005), pp.393-397.

[25] A. R. Waugh and M. J. Southon, *Surface analysis and grain-boundary segregation measurements using atom-prove techniques*, Surf. Sci. 89 (1979), pp.718-724.

[26] J. Takahashi, K. Kawakami, K. Ushioda, S. Takaki, N. Nakata, and T. Tsuchiyama, *Quantitative analysis of grain boundaries in carbon- and nitrogenadded ferritic steels by atom probe tomography*, Scripta Mater. 66 (2012), pp.207-210.

[27] Y. Zhang, G. -H. Lu, S. Deng and T. Wang, *Weakening of an aluminum grain boundary induced by sulfur segregation: A first-principles computational tensile test*, Phys. Rev. B 75 (2007), pp.174101.

[28] H. Momida, Y. Asari, Y. Nakamura, Y. Tateyama, and T. Ohno, *Hydrogen-enhanced vacancy embrittlement of grain boundaries in iron*, Phys. Rev. B 88 (2013), pp.144107.

[29] C. Molteni, G. P. Francis, M. C. Payne, and V. Heine, *First principles simulation of grain boundary sliding*, Phys. Rev. Lett. 76 (1996), pp.1284.

[30] C. Molteni, N. Marzari, M. C. Payne, and V. Heine, *Sliding mechanisms in aluminium grain boundaries*, Phys. Rev. Lett. 79 (1997), pp.869.

[31] J. -X. Shang and C. -Y. Wang, *Electronic effects of alloying elements Nb and V on body-centred-cubic Fe grain boundary cohesion*, J. Phys.: Condens. Matter 13 (2001) pp.9635-9644.

[32] J. -X. Shang, X. -D. Zhang, F. -H. Wang, C. -Y. Wang and H. -B. Xu, *Effects of Co and Cr on bcc Fe grain boundaries cohesion from first-principles study*, Comput. Mater. Science 38 (2006), pp.217-222.

[33] G. Duscher, M. R. Chisholm, U. Alber, and M. Ruhle, *Bismuth-induced embrittlement of copper grain boundaries*, Nature Mater. 3 (2004), pp.621-626.

[34] Y. -Q. Fen and C.-Y. Wang, *Electronic effects of nitrogen and phosphorus on iron grain boundary cohesion*, Comput. Mater. Sci. 20 (2001), pp.48-56.

[35] N. Kioussis, M. Herbranson, E. Collins, and M. E. Eberhart, *Topology of electronic charge density and energies of planar faults in fcc metals*, Phys. Rev. Lett. 88 (2002), pp.125501.

[36] M. E. Eberhart, D. P. Clougherty, and J. M. MacLaren, *A theoretical investigation of the mechanisms of fracture in metals and alloys*, J. Am. Chem. Soc. 115 (1993), pp.5762-5767.

[37] M. Yuasa and M. Mabuchi, *First-principles study in Fe grain boundary with Al segregation: variation in electronic structures with straining*, Phil. Mag. 93 (2013), pp.635-647.

[38] J. R. Rice and R. Thomson, *Ductile versus brittle behaviour of crystals*, Phil. Mag. 29 (1974), pp.73-97.

Acknowledgements

N. M. acknowledges support from a Grant-in-Aid for JSPS Fellows.

Disclosure statement

No potential conflict of interest was reported by the author.

Figure legends

Figure 1. Unit cell model of the C-segregated Fe Σ3 (111)/[$1\bar{1}0$] tilt GB segregated by C. C1 indicates a C atom, and Fe1, Fe2, Fe3 and Fe4 indicate Fe atoms around the C atom. C atoms are placed at interstitial sites on both sides of the Fe GB. The initial cells are 0.405 nm × 0.702 nm × 1.489 nm.

Figure 2. Results of first-principles fully relaxed tensile tests for clean and C-segregated GBs. (a) Total energy–strain curve and (b) stress–strain curve.

Figure 3. Charge density distribution for the ($1\bar{1}0$) plane in the C-segregated GB: (a) 0% strain, (b) 20% strain, (c) 22% strain, (d) 26% strain, and (e) 28% strain.

Figure 4. Partial densities of states of the C1 atom in the C-segregated GB: (a) 0% strain, (b) 20% strain, (c) 22% strain, (d) 26% strain, and (e) 28% strain.

Figure 5. Partial densities of states of Fe2 and Fe4 atoms in the C-segregated GB: (a) 0% strain, (b) 20% strain, (c) 22% strain, (d) 26% strain, (e) 28% strain for the Fe2 atom, and (f) 0% strain, (g) 20% strain, (h) 22% strain, (i) 26% strain, and (j) 28% strain for the Fe4 atom.

Figure 6. Partial densities of states of the P atom for the P-segregated GB: (a) 0% strain, (b) 4% strain, (c) 8% strain, (d) 10% strain, and (e) 12% strain. The P–Fe bond breaks at 10–12% strain.

Figure 7. Variation in the charge density along the line normal to the C1–Fe4 bond passing through the bond critical point (BCP) of C1–Fe4.

Figure 8. Variation in the total energy during sliding in the clean GB and C-segregated GB.

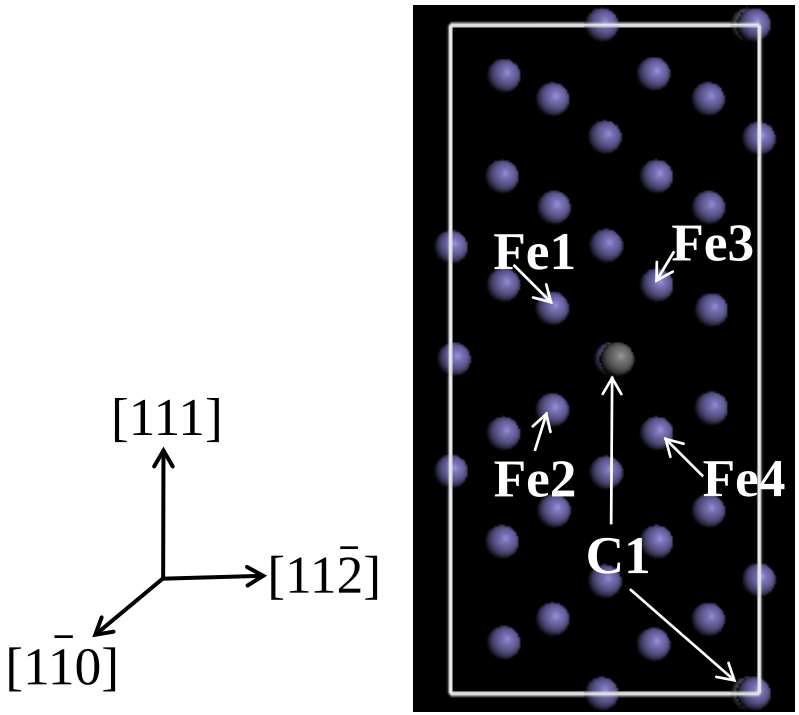

Figure 1

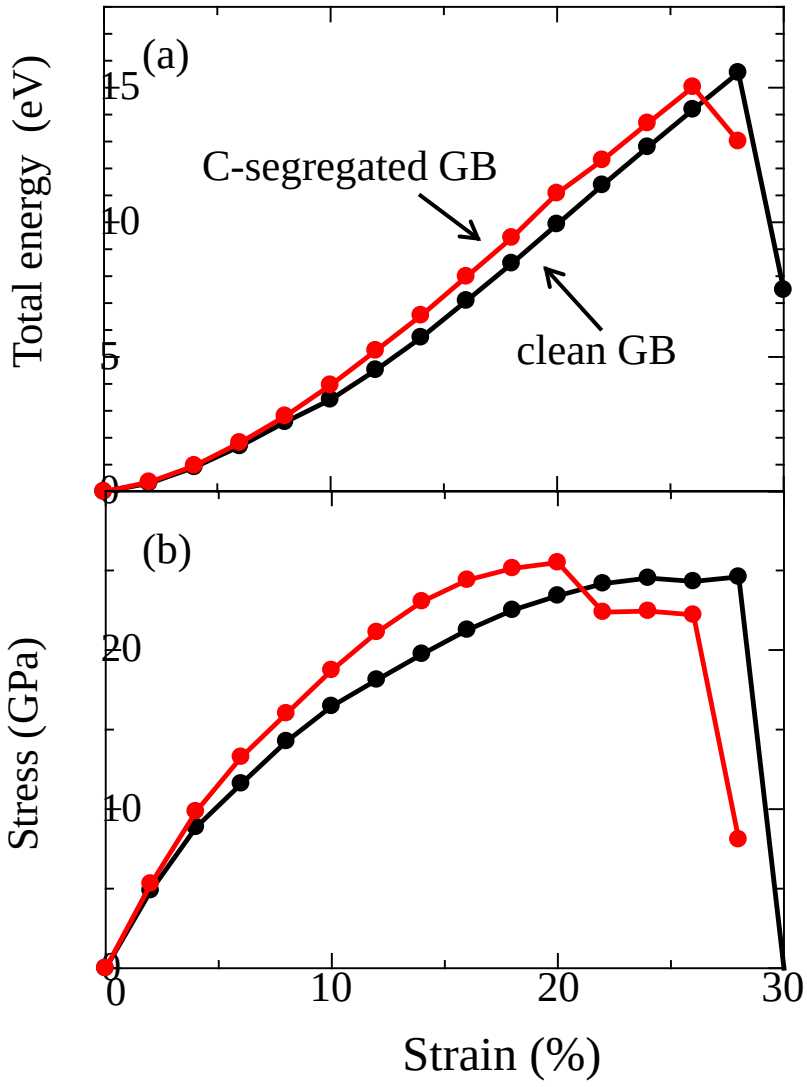
(a)
Total energy (eV)
C-segregated GB
clean GB
(b)
Stress (GPa)
Strain (%)
0
10
20
30

Figure 2

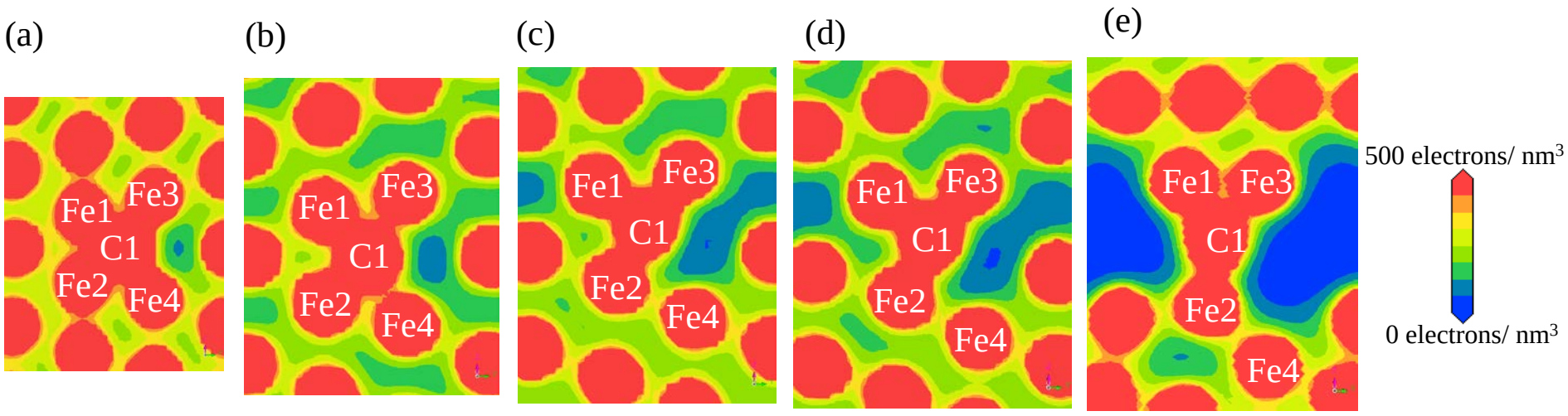

Figure 3

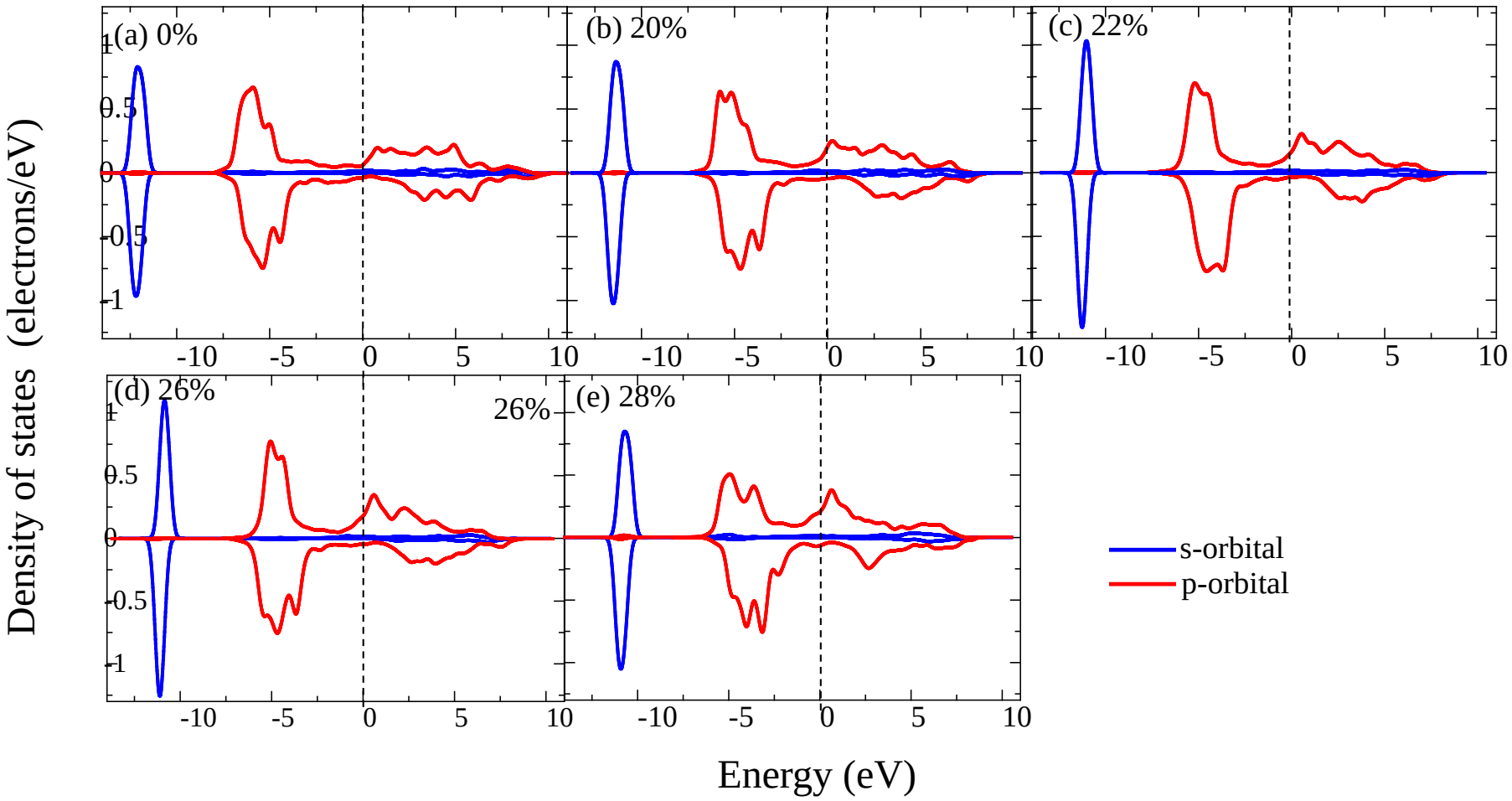
(a) 0%
(b) 20%
(c) 22%
(d) 26%
26%
(e) 28%
Density of states (electrons/eV)
Energy (eV)
s-orbital
p-orbital

Figure 4

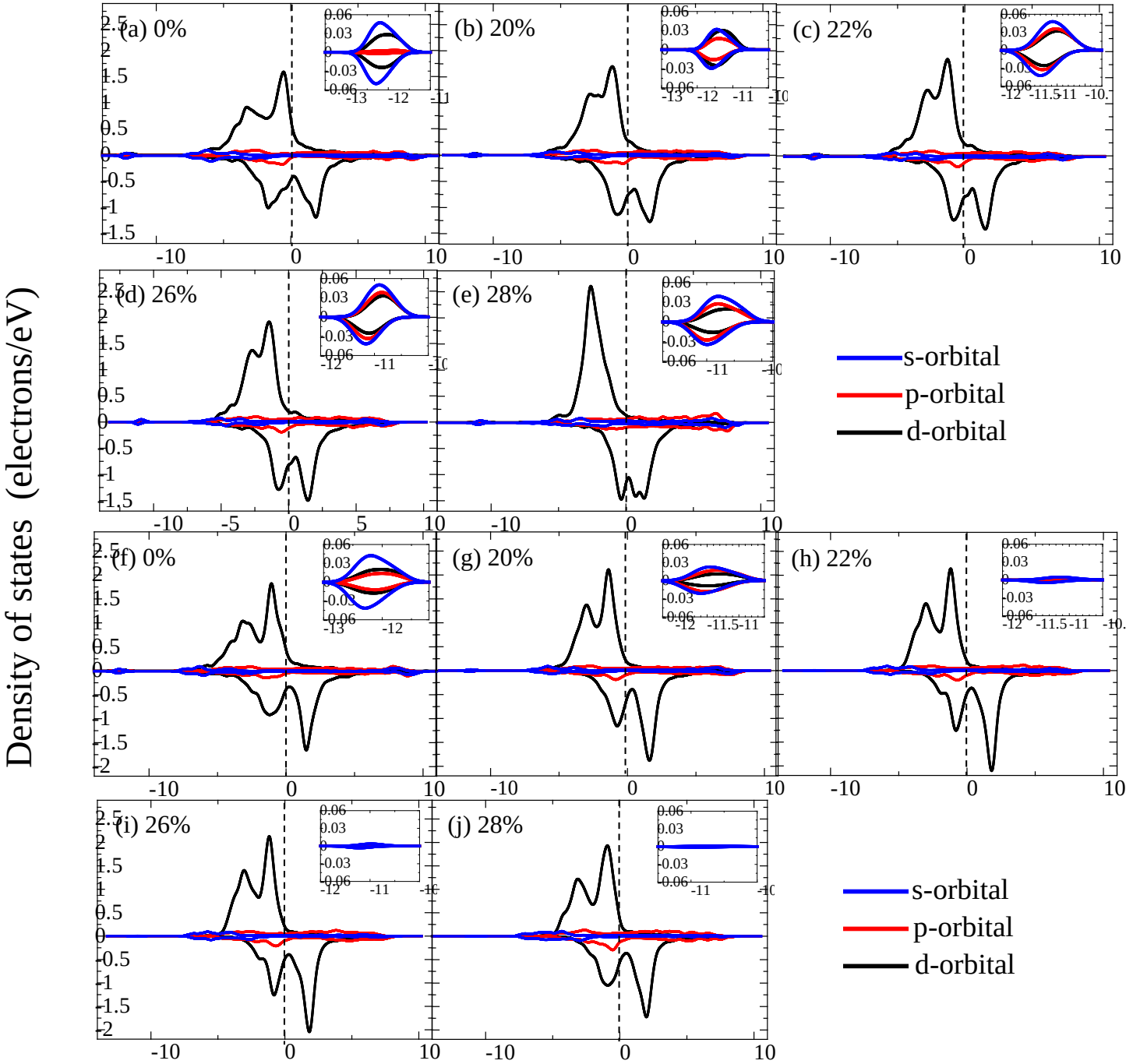
(a) 0%
(b) 20%
(c) 22%
(d) 26%
(e) 28%
(f) 0%
(g) 20%
(h) 22%
(i) 26%
(j) 28%
s-orbital
p-orbital
d-orbital
Density of states (electrons/eV)
Energy (eV)

Figure 5

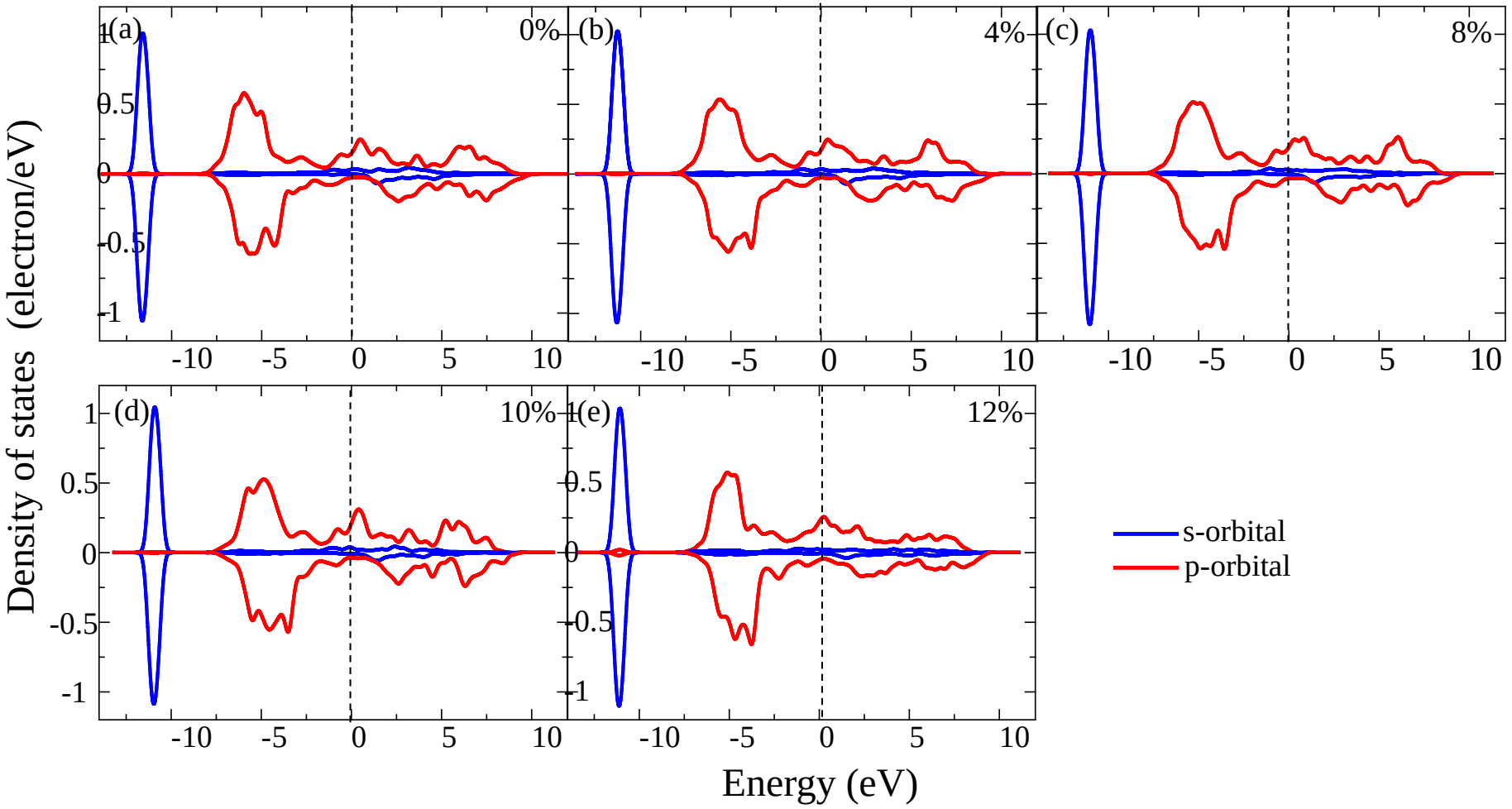
(a)
0%
(b)
4%
(c)
8%
(d)
10%
(e)
12%
Density of states (electron/eV)
Energy (eV)
s-orbital
p-orbital

Figure 6

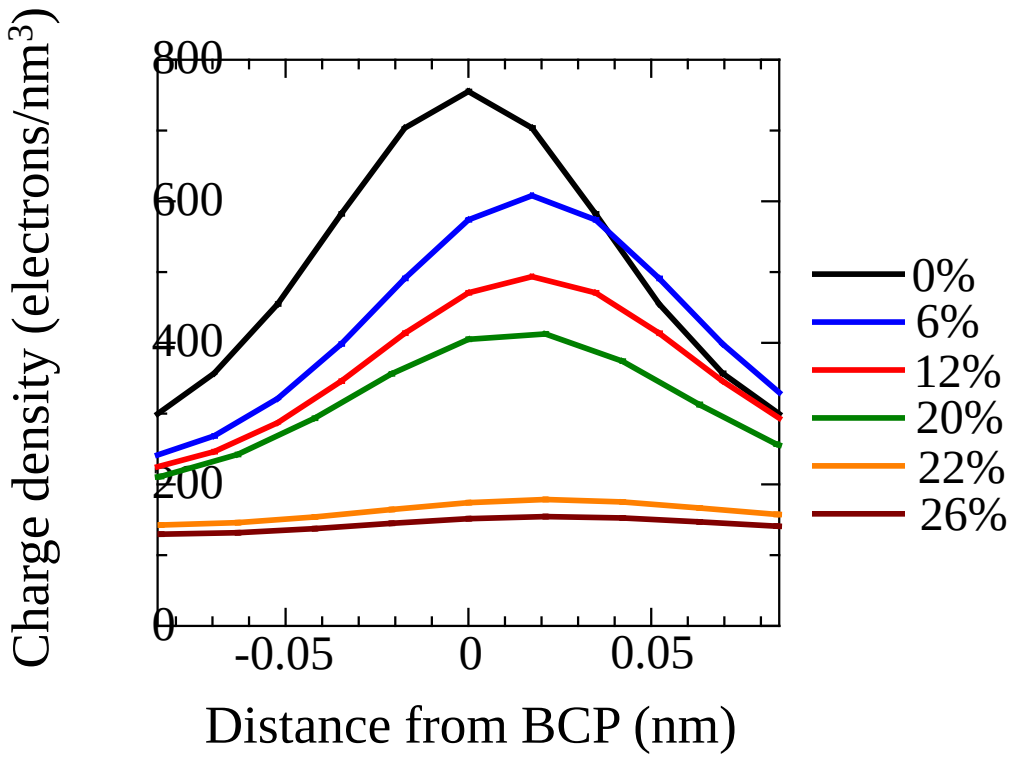
Charge density (electrons/nm3)
800
600
400
200
0
-0.05
0
0.05
Distance from BCP (nm)
0%
6%
12%
20%
22%
26%

Figure 7

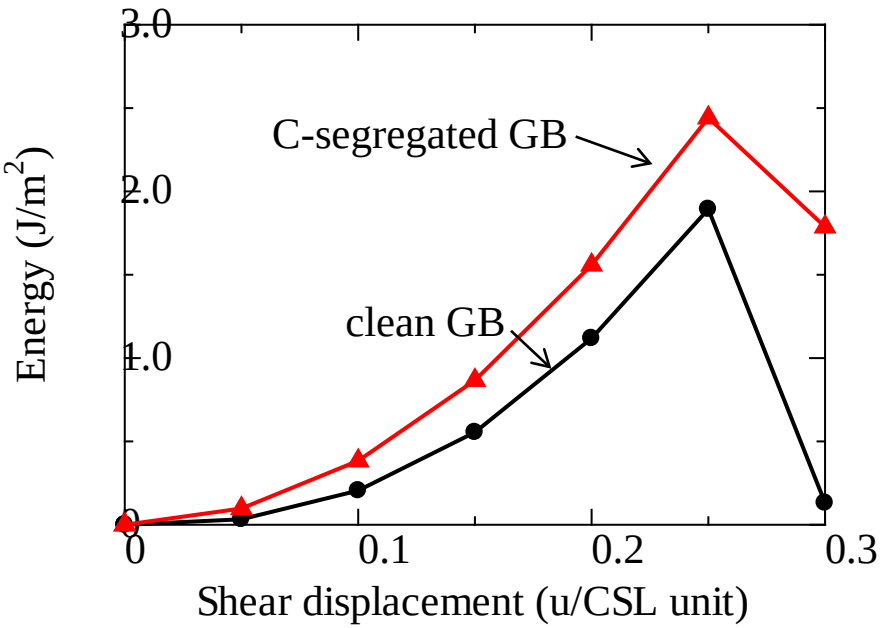
3.0
2.0
1.0
0
Energy (J/m^2)
C-segregated GB
clean GB
0
0.1
0.2
0.3
Shear displacement (u/CSL unit)

Figure 8